

Article

Synthesis of Chiral Helic[1]tritycene[3]arenes and Their Enantioselective Recognition towards Chiral Guests Containing Aminoindan Groups

Jing Li^{1,2}, Ying Han¹ and Chuan-Feng Chen^{1,2,*} 

¹ Beijing National Laboratory for Molecular Sciences, CAS Key Laboratory of Molecular Recognition and Function, Institute of Chemistry, Chinese Academy of Sciences, Beijing 100190, China; lijing2015@iccas.ac.cn (J.L.); hanying463@iccas.ac.cn (Y.H.)

² University of Chinese Academy of Sciences, Beijing 100049, China

* Correspondence: cchen@iccas.ac.cn; Tel.: +86-10-6258-8936

Abstract: Starting from the enantiopure precursors, a pair of chiral macrocyclic arenes named helic[1]tritycene[3]arenes were conveniently synthesized. The circular dichroism (CD) spectra of the enantiomeric macrocyclic arenes exhibited mirror images, and the X-ray single crystal structures confirmed their absolute conformations as well. Moreover, the macrocyclic arenes showed strong complexation with secondary ammonium and primary ammonium salts containing aminoindan groups. In particular, the chiral macrocyclic arenes exhibited enantioselective recognition ability towards the chiral secondary ammonium salts containing aminoindan groups with an enantioselective ratio up to 3.89.

Keywords: macrocyclic arene; enantioselective recognition; helic[1]tritycene[3]arene; ammonium salts



Citation: Li, J.; Han, Y.; Chen, C.-F. Synthesis of Chiral Helic[1]tritycene[3]arenes and Their Enantioselective Recognition towards Chiral Guests Containing Aminoindan Groups. *Molecules* **2021**, *26*, 536. <https://doi.org/10.3390/molecules26030536>

Academic Editors: Feihe Huang and Hiroyasu Yamaguchi
Received: 9 December 2020
Accepted: 18 January 2021
Published: 20 January 2021

Publisher's Note: MDPI stays neutral with regard to jurisdictional claims in published maps and institutional affiliations.



Copyright: © 2021 by the authors. Licensee MDPI, Basel, Switzerland. This article is an open access article distributed under the terms and conditions of the Creative Commons Attribution (CC BY) license (<https://creativecommons.org/licenses/by/4.0/>).

1. Introduction

Rasagiline is the second generation of monoamine oxidase inhibitor, which exhibits efficient capacity in blocking the breakdown of the neurotransmitter dopamine, and improving therapeutic effect on patients that suffered the decline in potency of long-term applications of dopamine [1]. Furthermore, the metabolite of rasagiline is an inactive non-benzedrinum with few side effects [2]. Azilect, namely rasagiline mesylate, is essentially a chiral secondary ammonium salt with excellent medicinal cure effects. However, there is little research into the recognition, and especially the enantioselective recognition, towards these bioactive guests based on synthetic receptors so far [3].

Macrocyclic arenes are a type of macrocycles which all composed of hydroxyl substituted aromatic rings bridged by methylene or methenyl groups [4]. Macrocyclic arenes have exhibited wide applications in host–guest chemistry [5–10], self-assembly [11,12], molecular machines [13], and material sciences [14–16]. Novel macrocyclic arenes have been reported successively in recent years to enrich the macrocyclic arene library [17]. Although the macrocyclic arene's recognition ability towards ammonium salts have been well studied [18–22], their enantioselective recognition towards ammonium salts, and especially those bioactive ammonium salts, have been rarely reported [23].

Previously, we [24] reported a new macrocyclic arene named helic[1]tritycene[3]arene that exhibited excellent recognition ability towards the organic ammonium salts. Since the protonated rasagiline and its metabolite were chiral ammonium salts, we deduced that enantiopure macrocyclic arenes based on the helic[1]tritycene[3]arene could show enantioselective recognition ability toward the chiral guests containing aminoindan groups. In this paper, we report a pair of enantiopure helic[1]tritycene[3]arenes *P-H* and *M-H*, which could be conveniently synthesized by one-pot reaction starting from the enantiopure precursors. *P-H* and *M-H* showed mirror CD spectra and they could also self-assemble into

herringbone-like architecture in the solid states. The enantiopure macrocycles exhibited enantioselective recognition abilities towards chiral secondary ammonium salts (*R/S*-G1) and primary ammonium salts (*R/S*-G2, Figure 1). In particular, the *P*-H showed high enantioselectivity towards *R*-G1 than *S*-G1 with the ratio up to 3.89:1.

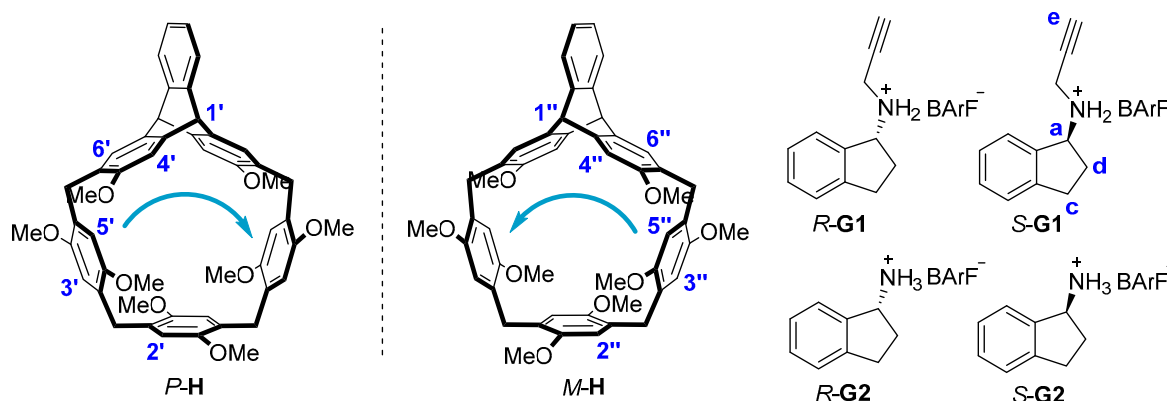
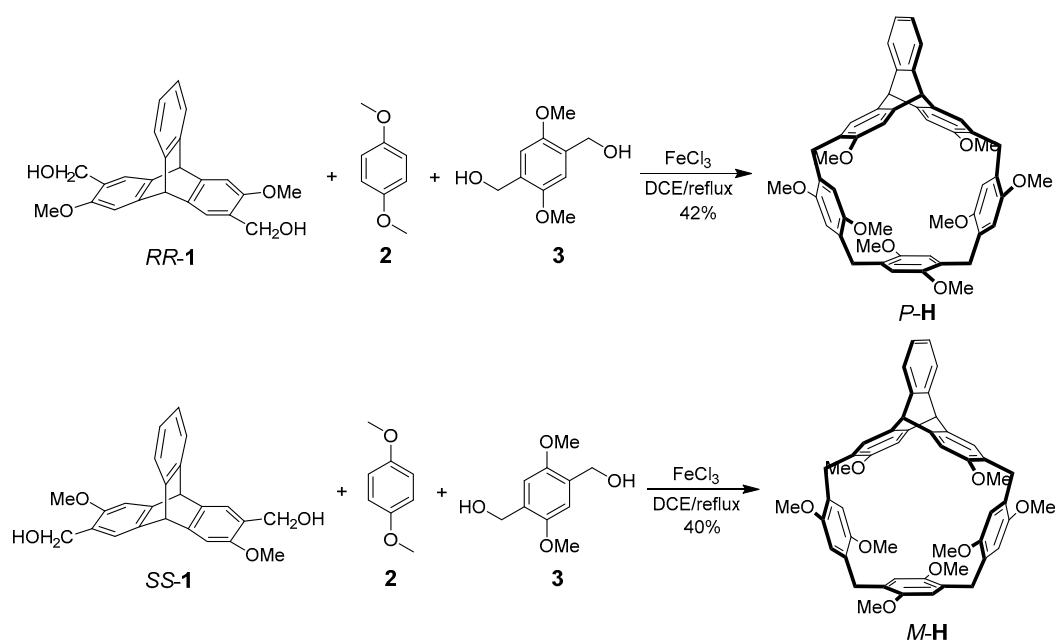


Figure 1. Structures and proton designations of the hosts (*P*-H/*M*-H) and the guests (*R*-G1/*S*-G1 and *R*-G2/*S*-G2).

2. Results and Discussion

2.1. Synthesis and Structures

Synthesis of enantiomeric helic[1]triptycene[3]arenes *P*-H/*M*-H was depicted in Scheme 1. *RR*-1 and *SS*-1 were first obtained by efficient chiral resolution of the racemic triptycene derivative with HPLC on chiral column (Figures S1–S3, in the Supplementary Materials). By the reaction of *RR*-1, 1,4-dimethoxybenzene **2** and 1,4-dihydroxymethyl-2,5-dimethoxybenzene **3** [25] with a catalytic amount of FeCl₃ in dichloroethane, we conveniently obtained *P*-H with 42% yield. Similarly, starting from *SS*-1 and **2** and **3**, we obtained *M*-H with 40% yield. *P*-H and *M*-H both exhibited good solubility in common solvents including chloroform, dichloromethane, dichloroethane and tetrahydrofuran. Starting from commercial materials, the guests were conveniently obtained by two-step reactions as well (see Materials and Methods for details).



Scheme 1. Synthetic Routes to *P*-H and *M*-H.

The specific rotation $[\alpha]_{\text{D}}^{25}$ of *RR-1* in dichloromethane was 21° . By cyclization reaction of *RR-1* with **2** and **3**, the resulting product *P-H* showed its $[\alpha]_{\text{D}}^{25}$ of 123° in dichloromethane, which was significantly bigger than that of *RR-1*. Similarly, the specific rotation $[\alpha]_{\text{D}}^{25}$ of *SS-1* in dichloromethane was -21° , while $[\alpha]_{\text{D}}^{25}$ of the macrocyclic arene *M-H* in dichloromethane was -128° . Moreover, the circular dichroism (CD) spectra of *P-H* and *M-H* showed mirror images (Figure 2), which confirmed their enantiomeric structures. The enantiopure hosts and guests were further characterized by their ^1H NMR, ^{13}C NMR and HRMS spectra.

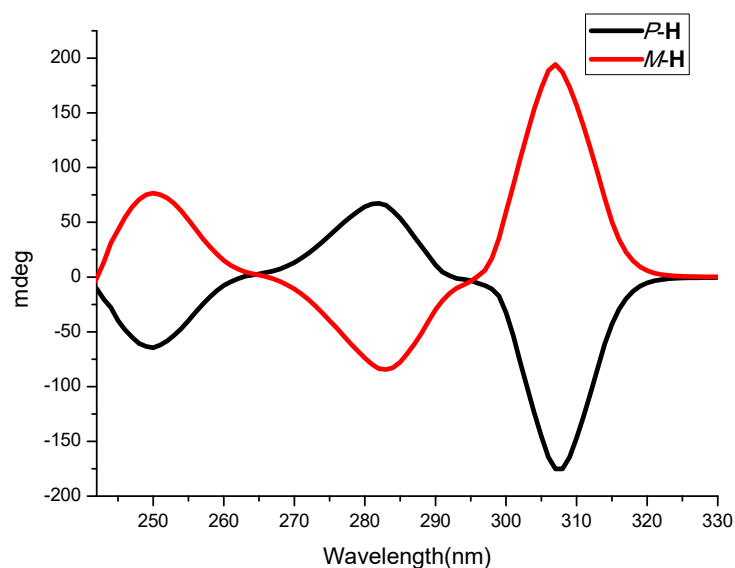


Figure 2. CD spectra of *P-H* and *M-H* (CH_2Cl_2 , $c = 2 \times 10^{-5} \text{ M}^{-1}$, $T = 298 \text{ K}$).

2.2. Crystal Structures

By slow evaporation of the macrocyclic hosts in mixture solution of dichloromethane and isopropyl ether at room temperature, we obtained the colorless single crystals. As shown in Figure 3, the macrocycles adopted the bucket-like structures with the mirror image correspondence. For *P-H*, the methoxy groups on one rim adopted the clockwise orientation, while for *M-H*, the methoxy groups on one rim adopted the anticlockwise orientation. This result was in accordance with their mirror images reflected in CD spectra. Moreover, one dichloromethane molecule was encapsulated in the center of the macrocyclic cavity. It was further found that both *P-H* and *M-H* could self-assemble into herringbone-like architectures along *c* axis while the orientations were different from each other (Figure 3c,d).

We also obtained the colorless single crystal of *P-H* by slow evaporation of acetonitrile and isopropyl ether solution at room temperature. As shown in Figure 4, one acetonitrile molecule was encapsulated in the center of the *P-H*'s cavity. There existed multiple $\text{C}-\text{H}\cdots\text{N}$ interactions between acetonitrile and the two adjacent macrocycles in the distance of 2.662 \AA for A, 2.736 \AA for B and 2.738 \AA for C, respectively. Since the encapsulated acetonitrile showed noncovalent interactions with the adjacent macrocycle, the two adjacent macrocycles were thus drawing closer compared with the macrocycle that encapsulated dichloromethane. There existed multiple $\text{C}-\text{H}\cdots\pi$ interactions (2.871 \AA for D and 2.858 \AA for E) and multiple $\text{C}-\text{H}\cdots\text{O}$ interactions (2.579 \AA for F, 2.667 \AA for G and 2.656 \AA for H) between the two adjacent macrocycles. Moreover, the macrocycles could pack in a herringbone pattern along the *c* axis in a more closely packed mode compared with the aforementioned macrocycle that encapsulated dichloromethane.

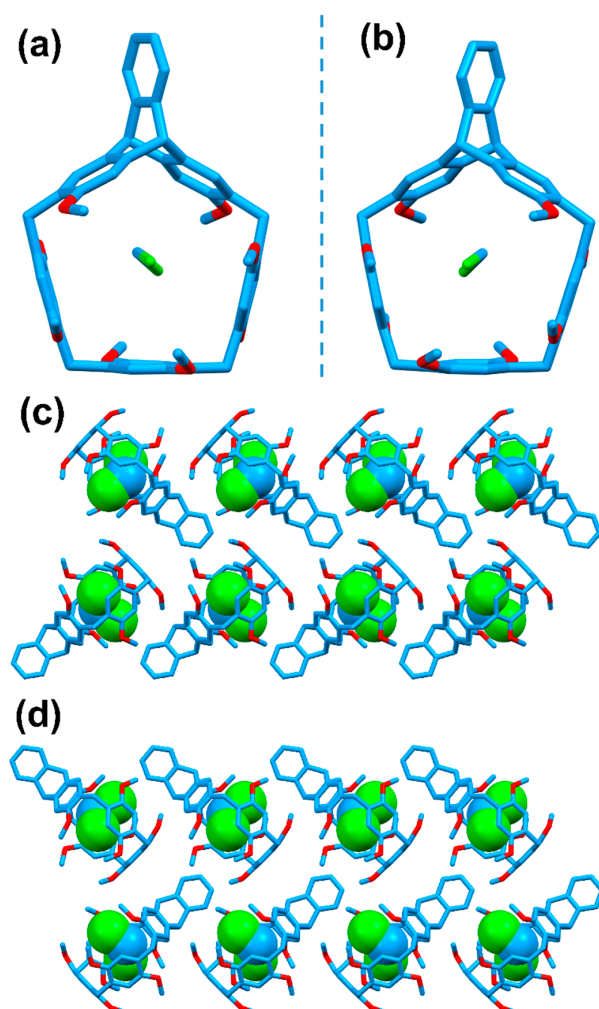


Figure 3. Crystal structures of (a) *P-H*, (b) *M-H* and packing mode of (c) *P-H*, (d) *M-H* along the *c* axis. Hydrogen atoms were omitted for clarity.

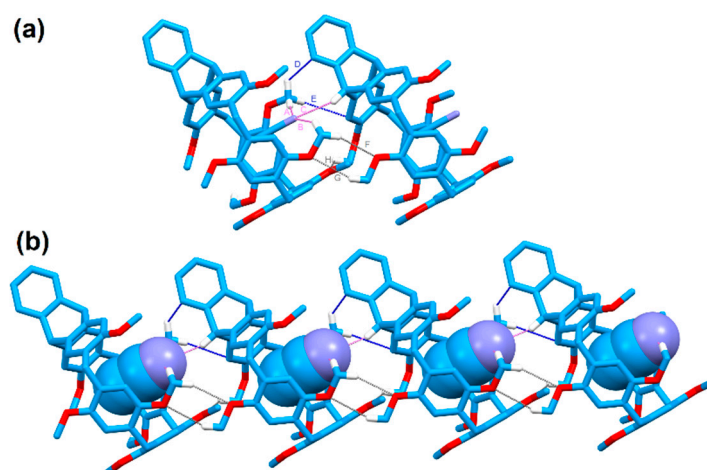


Figure 4. (a) Crystal structure and (b) packing mode along the *c* axis of *P-H*. Dotted lines denoted the noncovalent interactions between *P-H* and CH_3CN (violet for $\text{C-H}\cdots\text{N}$ interactions, grey for $\text{C-H}\cdots\text{O}$ interactions and blue for $\text{C-H}\cdots\pi$ interactions). Hydrogen atoms not involved in the noncovalent interactions were omitted for clarity.

2.3. Enantioselective Recognition Ability of the Macrocyclic Hosts towards Ammonium Salts

To investigate the enantioselective complexation of enantiomeric helic[1]tritycene[3]arenes *P-H*/*M-H*, two pairs of enantiopure bioactive ammonium salts containing aminocandans groups have been chosen as the guests. *R-G1* is the protonated derivative of rasagiline, which is an important monoamine oxidase inhibitor [1]. *R-G2* is the protonated derivative of the metabolite of rasagiline, which is an inactive non-benzedrinum with few side effects [2].

Firstly, we tested the enantioselective recognition ability towards the guests by the racemic host through ^1H NMR spectra. When *R-G1* was added into *rac-H* in CDCl_3 solution, a new set of proton signals which were different from those of the free host and the free guest appeared, indicating the host-guest complexation was the fast exchange process in NMR timescale (Figure 5). When *R-G1* was added into the host's solution, the proton signal of H_1 of *rac-H* split. With the increasing amount of *R-G1* into the host's solution, the splitting trend was even greater. The proton signal of H_2 of *rac-H* also split after the addition of *R-G1* into the host's solution. These phenomena indicated that helic[1]tritycene[3]arene showed enantioselective recognition ability towards *G1*. Similarly, upon addition of *R-G2* into *rac-H* in CD_2Cl_2 solution, the proton signals of *rac-H* also split (Figure S20, in the Supplementary Materials), which confirmed the chiral recognition ability of the macrocycle towards *G2*.

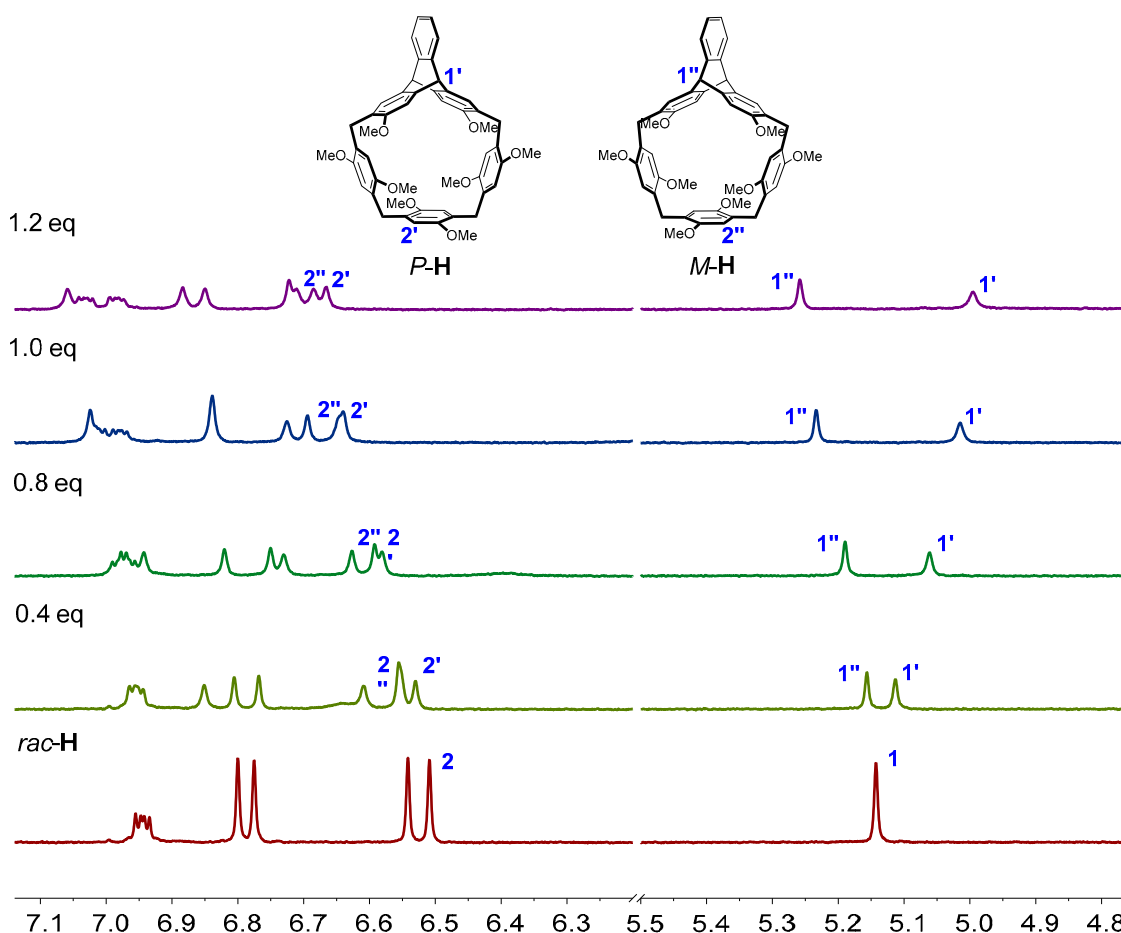


Figure 5. Partial ^1H NMR spectra (400MHz, 298 K, CDCl_3) of 2.0 mM *rac-H* with different amounts of *R-G1*.

The host-guest complexations between *P-H*/*M-H* and the chiral guests were then investigated by ^1H NMR spectroscopy. When equimolar *M-H* and *S-G1* were mixed in CDCl_3 solution, a new set of proton signals different from free host and free guest appeared, suggesting the complexation was fast exchange process in NMR timescale (Figure 6). The

proton signals of H_1'' and H_4'' of *M-H* showed upfield shifts while other proton signals of *M-H* showed downfield shifts. The proton signals of H_a-H_e of *S-G1* all showed upfield shifts probably due to the shielding effect of *M-H*. Other host-guest complexes also showed similar complexation mode and the complexations were all fast exchange processes in NMR timescale (Figures S21–S28, in the Supplementary Materials). Besides, the CD spectra of the enantiomeric hosts in the presence of the guests exhibited mirror images as well (Figure S72, in the Supplementary Materials). Compared with the individual hosts, the CD spectra of the host-guest complexes exhibited slight enhanced cotton effects at 248, 288, and 308 nm.

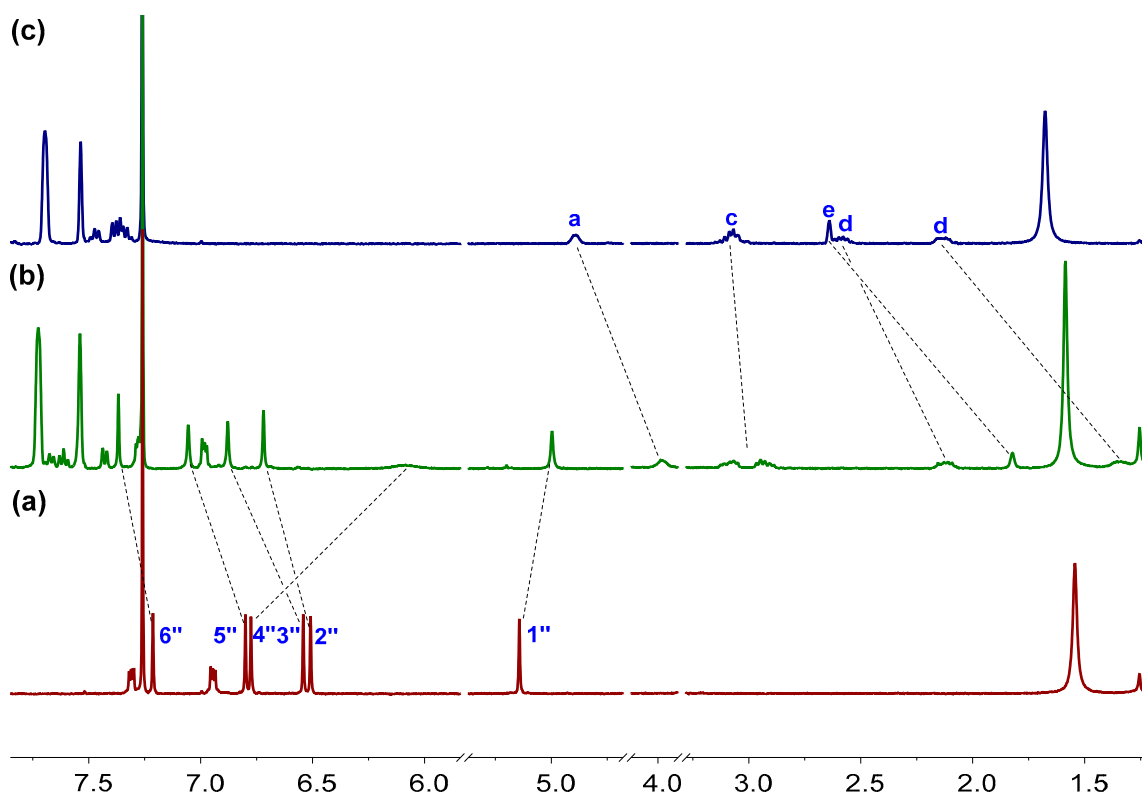


Figure 6. Partial ^1H NMR spectra (500 MHz, 298 K, CDCl_3) of (a) *M-H*, (b) *M-H* + 1.0 equiv. *S-G1*, (c) *S-G1*. $[M-H]_0 = 3.0$ mM.

In order to quantitatively study the complexation strength between the hosts and the guests, ^1H NMR titration experiments were performed, and the association constants were calculated by the non-linear fitting method [26]. The complex-ratios were all calculated to be 1:1 through Job plot method (Figures S37, S40, S43, S46, S49, S52, S55 and S58, in the Supplementary Materials), and the association constants were summarized in Table 1. The association constants between the hosts and the secondary ammonium salts were in the vicinity of 10^3 M^{-1} in chloroform. *P-H* showed biggest association constant with *R-G1* in the value of $(7.63 \pm 0.75) \times 10^3 \text{ M}^{-1}$. Meanwhile, *P-H* showed moderate association constant with *S-G1* in the value of $(1.96 \pm 0.18) \times 10^3 \text{ M}^{-1}$. It's noteworthy that the association constant of *P-H* towards *R-G1* was 3.89 times of *P-H* towards *S-G1*. The association constants between the hosts and the primary ammonium salts were in the vicinity of 10^2 M^{-1} in dichloromethane. And the association constant of *P-H* towards *R-G2* was 1.61 times of *P-H* towards *S-G2*.

HRMS analysis also confirmed the 1:1 complexation ratio of those host-guest complexes in gas phase. The strongest peak at m/z 948.4447 for $[P-H \cdot R-G1 \cdot \text{BArF}]^+$ was found by using a solution of *P-H* and *R-G1* in chloroform, which was in accordance with formation of the 1:1 complex in solution. Similarly, the strongest peaks at m/z 948.4444, 948.4446, 948.4442, 910.4316, 910.4319, 910.4323, and 910.4319 for $[P-H \cdot S-G1 \cdot \text{BArF}]^+$, $[M-H \cdot R-G1 \cdot \text{BArF}]^+$, $[M-H \cdot S-G1 \cdot \text{BArF}]^+$, $[P-H \cdot R-G2 \cdot \text{BArF}]^+$, $[P-H \cdot S-G2 \cdot \text{BArF}]^+$, $[M-H \cdot R-G2 \cdot \text{BArF}]^+$,

$[M\text{-H}\cdot S\text{-G2}\text{-BArF}]^+$ were also observed, respectively (Figures S29–S36, in the Supplementary Materials), which further verified formation of the 1:1 complexes.

Table 1. Association Constants (K_a/M^{-1}) for 1:1 Complexes Between Chiral **H** and Chiral **G1–G2** at 298 K.

Guests	<i>P</i> - H		<i>M</i> - H	
	$K_a M^{-1}$	K_R/K_S	$K_a M^{-1}$	K_R/K_S
<i>R</i> - G1 ¹	$(7.63 \pm 0.75) \times 10^3$	3.89/1	$(2.10 \pm 0.20) \times 10^3$	1/3.28
<i>S</i> - G1 ¹	$(1.96 \pm 0.18) \times 10^3$		$(6.98 \pm 0.67) \times 10^3$	
<i>R</i> - G2 ²	$(3.44 \pm 0.32) \times 10^2$	1.61/1	$(2.06 \pm 0.19) \times 10^2$	1/1.40
<i>S</i> - G2 ²	$(2.14 \pm 0.19) \times 10^2$		$(2.88 \pm 0.27) \times 10^2$	

¹ In CDCl₃. ² In CD₂Cl₂.

2.4. DFT and IGM Analyses of Complexes *P*-**H**·*R*-**G1** and *P*-**H**·*S*-**G1**

To further investigate the enantioselective recognition of the chiral macrocycles towards *R*-**G1** and *S*-**G1**, DFT calculations for the host-guest complexes without consideration of the counter anions were carried out by using B3LYP/6-31G(d) method [27]. As shown in Figure 7, the alkynyl group and ammonium group of the guests were both located inside the cavity of *P*-**H**, while the indane group was outside the cavity. According to the superimposed views of optimized structures for the complexes *P*-**H**·*R*-**G1** and *P*-**H**·*S*-**G1**, the main difference for the complexes lay in the noncovalent interactions between the chiral center of the guests and the methoxy group at the rim of the host. For complex *P*-**H**·*R*-**G1**, the C-H···O hydrogen bonds between the hydrogen of the chiral carbon of *R*-**G1** and the oxygen at the rim of the triptycene unit was in the distance of 2.7 Å. For complex *P*-**H**·*S*-**G1**, the C-H···O hydrogen bonds between the hydrogen of the chiral carbon of *S*-**G1** and the oxygen at the rim of the phenyl unit was in the distance of 3.2 Å, which was essentially weak noncovalent interactions compared with *P*-**H**·*R*-**G1** [28]. Moreover, complex *P*-**H**·*R*-**G1** showed lower energy ($-13.0 \text{ kcal mol}^{-1}$) than that of *P*-**H**·*S*-**G1** ($-12.1 \text{ kcal mol}^{-1}$), which indicated that complex *P*-**H**·*R*-**G1** was thermodynamically stable adduct than complex *P*-**H**·*S*-**G1** (Table S8, in the Supplementary Materials). This was consistent with the result of *P*-**H**'s preference for *R*-**G1** over *S*-**G1**.

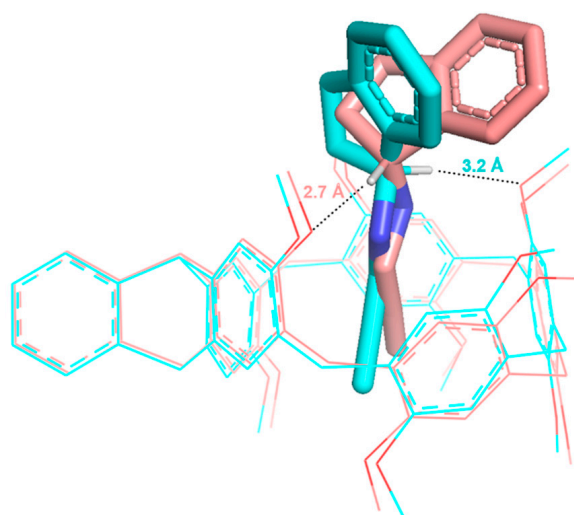


Figure 7. Superimposed views of optimized structures for the complexes between host *P*-**H** and the enantiomers *R*-**G1**/*S*-**G1**. Pink and light blue denote guests *R*-**G1** and *S*-**G1**, respectively. Dotted lines denote the C-H···O hydrogen bonds in the host-guest complexes.

Moreover, IGM [29] analyses for complexes *P*-**H**·*R*-**G1** and *P*-**H**·*S*-**G1** were also carried out based on their optimal structures. As shown in Figure 8, there existed not only the

dispersion force (the green region) but also multiple C–H $\cdots\pi$ interactions and N–H \cdots O and C–H \cdots O hydrogen binding interactions (the blue region) between *P-H* and *R-G1*, thus generating the strong interactions in this host-guest complex. For *P-H*·*S-G1*, there existed weak noncovalent intermolecular interactions in the host-guest complex, which might result in the lower association constant for *P-H*·*S-G1* compared with that of *P-H*·*R-G1*.

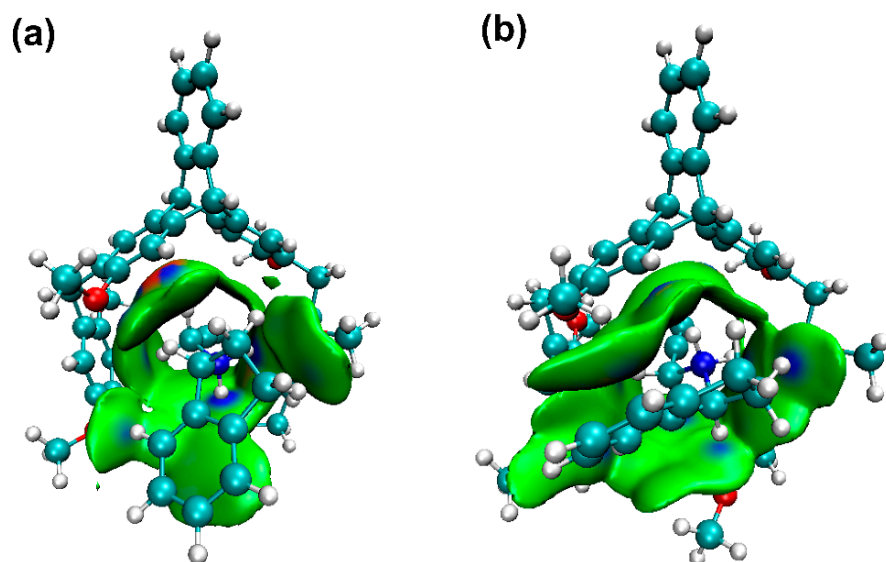


Figure 8. IGM analyses of the complexes (a) *P-H*·*R-G1*, (b) *P-H*·*S-G1* ($\delta_{\text{ginter}} = 0.002$).

3. Conclusions

In summary, we have conveniently synthesized a pair of enantiopure helic[1]tritycene arenes by one-pot reaction. The CD spectra of the chiral macrocycles showed mirror images, and X-ray crystal structures showed that one dichloromethane or acetonitrile molecule could be encapsulated in the cavities of the macrocycles, while the macrocyclic molecules could pack into the herringbone-like architectures along the *c* axis. Moreover, the macrocycles exhibited strong complexation with the bioactive guests containing aminoindan groups. It was further found that the chiral macrocyclic hosts showed enantioselective recognition ability towards chiral guests *G1* and *G2*. In particular, *P-H* showed preference for *R-G1* over *S-G1* with an enantioselective ratio up to 3.89. The selectivity might originate from the noncovalent interactions between the chiral carbon center of the guests and the methoxy groups at the rim of the hosts.

4. Materials and Methods

4.1. General Methods

All the reagents were commercially available and used without further purification. Reactions were carried out under inert and anhydrous conditions unless otherwise noted. Anhydrous solvents were dried from 4 Å molecular sieves. Flash column chromatography was performed on 200–300 mesh silica gel. ^1H and ^{13}C NMR spectra were measured at 298 K. The ionization methods used in mass spectrometry were atmospheric pressure chemical ionization (APCI) and electrospray ionization (ESI). Melting points, taken on an electrothermal melting point apparatus, were uncorrected. X-Ray single crystal data were measured by XtaLAB Synergy-R at 170 K. Circular dichroism spectra were measured by J-810 at 298 K.

4.2. General Synthesis Procedure for the Hosts

To a solution of *RR-1* (1.00 g, 2.65 mmol), **2** (0.75 g, 5.30 mmol), and **3** (0.55 g, 2.65 mmol) in dichloroethane (400 mL) was added FeCl_3 (0.05 g, 0.25 mmol). Then the mixture was refluxed in the oil bath under argon atmosphere for 12 h. After cooling to room temperature,

the mixture was evaporated under vacuum and the residue was further purified by flash column chromatography on silica gel (eluent: petroleum ether/ethyl acetate = 4:1, R_f = 0.4) to afford *P-H* as white solid (0.85 g, 42%).

According to the above method, *M-H* was obtained as white solid in 40% yield.

4.3. General Synthesis Procedure for the Guests

To the solution of (*R*)-*N*-(2-Propynyl)-2,3-dihydroinden-1-amine (171.2 mg, 1.0 mmol) in DCM (5 mL) was added excessive hydrochloric acid. The mixture was stirred for 30 min under room temperature and then filtrated to collect the residue. Then the residue was dissolved in DCM/H₂O (1:1, *v/v*, 10 mL) and sodium tetrakis [3,5-bis(trifluoromethyl)phenyl] borate (NaBARF) (886.2 mg, 1.0 mmol) was added subsequently. The mixture was stirred for 2 h under room temperature and then extracted with CH₂Cl₂. The organic phase was dried with MgSO₄, and concentrated to give *R-G1* (994.1 mg, 96%) as the white solid.

According to the similar method, *S-G1* was prepared as white solid in 97% yield, *R-G2* was prepared as white solid in 98% yield, and *S-G2* was prepared as white solid in 96% yield.

4.4. Characterization Data

RR-1.

¹H NMR (300 MHz, CDCl₃): δ 7.35–7.32 (m, 2H), 7.29 (s, 2H), 6.99 (s, 2H), 6.98–6.93 (m, 2H), 4.56 (s, 4H), 3.81 (s, 6H), 2.07 (s, 2H). ¹³C NMR (75 MHz, CDCl₃): δ 155.0, 147.0, 145.4, 137.4, 125.2, 124.9, 124.1, 123.3, 107.1, 61.9, 55.6, 53.6. M.p.: 156.7–159.8 °C. $[\alpha]_D^{25} = +21^\circ$ (*c* = 0.25, CH₂Cl₂). HRMS (APCI) *m/z*: [M-H]⁺ calcd for C₂₄H₂₁O₄[−] 373.1434; found 373.1429.

SS-1.

¹H NMR (400 MHz, CDCl₃): δ 7.33 (dd, *J* = 5.3, 3.2 Hz, 2H), 7.29 (s, 2H), 7.00–6.97 (m, 2H), 6.97–6.92 (m, 2H), 4.55 (s, 4H), 3.78 (s, 6H), 2.10 (s, 2H). ¹³C NMR (100 MHz, CDCl₃): δ 154.9, 147.0, 145.5, 137.5, 125.2, 125.0, 124.1, 123.3, 107.1, 61.8, 55.6, 53.6. M.p.: 159.2–161.6 °C. $[\alpha]_D^{25} = -21^\circ$ (*c* = 0.25, CH₂Cl₂). HRMS (APCI) *m/z*: [M-H]⁺ calcd for C₂₄H₂₁O₄[−] 373.1434; found 373.1428.

P-H.

¹H NMR (400 MHz, CDCl₃): δ 7.32–7.30 (m, 2H), 7.21 (s, 2H), 6.96–6.93 (m, 2H), 6.80 (s, 2H), 6.78 (s, 2H), 6.54 (s, 2H), 6.51 (s, 2H), 5.14 (s, 2H), 3.81 (d, *J* = 12.9 Hz, 2H), 3.75 (s, 4H), 3.69 (s, 6H), 3.64 (d, *J* = 12.9 Hz, 2H), 3.51 (s, 6H), 3.48 (s, 6H), 3.39 (s, 6H). ¹³C NMR (125 MHz, CDCl₃): δ 154.0, 151.0, 150.9, 145.7, 145.2, 137.3, 129.0, 128.8, 128.5, 126.3, 125.9, 124.8, 123.1, 114.5, 114.5, 114.1, 106.9, 56.1, 56.0, 55.9, 55.3, 53.4, 29.9, 29.6. M.p.: 221.8–223.9 °C. $[\alpha]_D^{25} = +123^\circ$ (*c* = 0.25, CH₂Cl₂). HRMS (ESI) *m/z*: [M+Na]⁺ calcd for C₅₀H₄₈O₈Na⁺ 799.3241; found 799.3252.

M-H.

¹H NMR (500 MHz, CDCl₃): δ 7.32–7.30 (m, 2H), 7.21 (s, 2H), 6.95–6.94 (m, 2H), 6.80 (s, 2H), 6.77 (s, 2H), 6.54 (s, 2H), 6.51 (s, 2H), 5.14 (s, 2H), 3.81 (d, *J* = 12.9 Hz, 2H), 3.76 (s, 4H), 3.68 (s, 6H), 3.64 (d, *J* = 13.0 Hz, 2H), 3.51 (s, 6H), 3.47 (s, 6H), 3.39 (s, 6H). ¹³C NMR (125 MHz, CDCl₃): δ 154.0, 151.0, 150.9, 145.7, 145.2, 137.3, 129.0, 128.8, 128.5, 126.3, 125.9, 124.8, 123.1, 114.5, 114.5, 114.1, 106.9, 56.1, 56.0, 55.9, 55.3, 53.4, 29.9, 29.6. M.p.: 219.8–221.2 °C. $[\alpha]_D^{25} = -128^\circ$ (*c* = 0.25, CH₂Cl₂). HRMS (ESI) *m/z*: [M+Na]⁺ calcd for C₅₀H₄₈O₈Na⁺ 799.3241; found 799.3221.

R-G1.

¹H NMR (400 MHz, CDCl₃): δ 7.72 (s, 8H), 7.56 (s, 4H), 7.52–7.48 (m, 1H), 7.44–7.30 (m, 3H), 7.02 (s, 2H), 4.93 (d, *J* = 6.7 Hz, 1H), 3.79–3.78 (m, 2H), 3.11–3.07 (m, 2H), 2.67 (t, *J* = 2.5 Hz, 1H), 2.65–2.55 (m, 1H), 2.16–2.12 (m, 1H). ¹³C{¹H} NMR (100 MHz, CDCl₃): δ 161.7 (q, ¹J_{CB} = 50 Hz), 144.4, 134.8, 133.3, 132.1, 129.0 (q, ²J_{CF} = 32 Hz), 128.3, 126.5, 124.9, 124.6 (q, ¹J_{CF} = 271 Hz), 117.6, 80.3, 70.5, 64.3, 35.7, 29.6, 29.2. M.p.: 81.8–82.9 °C.

$[\alpha]_{\text{D}}^{25} = +4^{\circ}$ ($c = 0.25$, CH_2Cl_2). HRMS (ESI) m/z : $[\text{M-BArF}]^+$ calcd for $\text{C}_{12}\text{H}_{14}\text{N}^+$ 172.1121; found 172.1118.

S-G1.

^1H NMR (400 MHz, CDCl_3): δ 7.72 (s, 8H), 7.56 (s, 4H), 7.49–7.42 (m, 1H), 7.38 (d, $J = 8.5$ Hz, 2H), 7.32 (t, $J = 7.5$ Hz, 1H), 4.92 (dd, $J = 7.5, 2.4$ Hz, 1H), 3.80 (d, $J = 2.6$ Hz, 2H), 3.15–3.00 (m, 2H), 2.63 (t, $J = 2.8$ Hz, 1H), 2.59–2.56 (m, 1H), 2.19–2.12 (m, 1H). $^{13}\text{C}\{^1\text{H}\}$ NMR (100 MHz, CDCl_3): δ 161.7 (q, $^1J_{\text{CB}} = 50$ Hz), 144.4, 134.8, 133.3, 132.0, 128.9 (q, $^2J_{\text{CF}} = 31$ Hz), 128.3, 126.5, 124.8, 124.6 (q, $^1J_{\text{CF}} = 271$ Hz), 117.6, 80.3, 70.6, 64.2, 35.7, 29.6, 29.2. M.p.: 78.9–80.7 °C. $[\alpha]_{\text{D}}^{25} = -3^{\circ}$ ($c = 0.25$, CH_2Cl_2). HRMS (ESI) m/z : $[\text{M-BArF}]^+$ calcd for $\text{C}_{12}\text{H}_{14}\text{N}^+$ 172.1121; found 172.1119.

R-G2.

^1H NMR (500 MHz, CD_2Cl_2): δ 7.74 (s, 8H), 7.58 (s, 4H), 7.48 (t, $J = 7.5$ Hz, 1H), 7.42 (d, $J = 7.5$ Hz, 2H), 7.37 (t, $J = 7.5$ Hz, 1H), 6.31–5.98 (m, 3H), 5.20–5.17 (m, 1H), 3.26–3.10 (m, 2H), 2.80–2.75 (m, 1H), 2.26–2.18 (m, 1H). $^{13}\text{C}\{^1\text{H}\}$ NMR (125 MHz, CD_2Cl_2): δ 163.1 (q, $^1J_{\text{CB}} = 50$ Hz), 145.6, 136.2, 135.6, 133.4, 130.2 (q, $^2J_{\text{CF}} = 31$ Hz), 129.8, 127.8, 126.0 (q, $^1J_{\text{CF}} = 270$ Hz), 125.4, 118.9, 62.1, 32.1, 31.0. M.p.: 66.5–67.5 °C. $[\alpha]_{\text{D}}^{25} = +3^{\circ}$ ($c = 0.25$, CH_2Cl_2). HRMS (ESI) m/z : $[\text{M-BArF}]^+$ calcd for $\text{C}_9\text{H}_{12}\text{N}^+$ 134.0964; found 134.0965.

S-G2.

^1H NMR (500 MHz, CD_2Cl_2): δ 7.74 (s, 8H), 7.58 (s, 4H), 7.48 (t, $J = 7.2$ Hz, 1H), 7.41 (d, $J = 8.3$ Hz, 2H), 7.37 (t, $J = 7.4$ Hz, 1H), 5.68 (s, 3H), 5.17 (d, $J = 7.3$ Hz, 1H), 3.27–3.08 (m, 2H), 2.86–2.69 (m, 1H), 2.27–2.14 (m, 1H). $^{13}\text{C}\{^1\text{H}\}$ NMR (125 MHz, CD_2Cl_2): δ 163.1 (q, $^1J_{\text{CB}} = 50$ Hz), 145.6, 136.2, 135.8, 133.4, 130.2 (q, $^2J_{\text{CF}} = 31$ Hz), 129.8, 127.8, 126.0 (q, $^1J_{\text{CF}} = 270$ Hz), 125.4, 118.9, 62.2, 32.2, 31.0. M.p.: 68.1–69.4 °C. $[\alpha]_{\text{D}}^{25} = -3^{\circ}$ ($c = 0.25$, CH_2Cl_2). HRMS (ESI) m/z : $[\text{M-BArF}]^+$ calcd for $\text{C}_9\text{H}_{12}\text{N}^+$ 134.0964; found 134.0963.

Supplementary Materials: The following are available online: HPLC charts, NMR spectra of new compounds, high resolution mass spectra for the complexes, determination of association constants for the complexes, CD spectra of the complexes, crystal structures and DFT calculations.

Author Contributions: Conceptualization, C.-F.C.; investigation, J.L.; supervision, C.-F.C. and Y.H.; funding acquisition, C.-F.C. and Y.H. All authors have read and agreed to the published version of the manuscript.

Funding: We thank the National Natural Science Foundation of China (91856117, 22031010 and 21772205) for financial support.

Informed Consent Statement: Informed consent was obtained from all subjects involved in the study.

Data Availability Statement: The data presented in this study are openly available in the article and Supplementary Materials.

Conflicts of Interest: The authors declare no conflict of interest.

References

1. Rascol, O.; Brooks, D.J.; Melamed, E.; Oertel, W.; Poewe, W.; Stocchi, F.; Tolosa, E.; LARGO Study Group. Rasagiline as an adjunct to levodopa in patients with Parkinson's disease and motor fluctuations (LARGO, Lasting effect in Adjunct therapy with Rasagiline Given Once daily, study): A randomised, double-blind, parallel-group trial. *Lancet* **2005**, *365*, 947–954. [[CrossRef](#)]
2. Hubálek, F.; Binda, C.; Li, M.; Herzig, Y.; Sterling, J.; Youdim, M.B.H.; Mattevi, A.; Edmondson, D.E. Inactivation of purified human recombinant monoamine oxidases A and B by rasagiline and its analogues. *J. Med. Chem.* **2004**, *47*, 1760–1766. [[CrossRef](#)] [[PubMed](#)]
3. Tak, K.M.; Park, E.J.; Hyun, M.H. Liquid chromatographic resolution of racemic rasagiline and its analogues on a chiral stationary phase based on (+)-(18-crown-6)-2,3,11,12-tetracarboxylic acid. *J. Sep. Sci.* **2013**, *36*, 3682–3687. [[CrossRef](#)] [[PubMed](#)]
4. Chen, C.-F.; Han, Y. Triptycene-derived macrocyclic arenes: From calixarenes to helicarenes. *Acc. Chem. Res.* **2018**, *51*, 2093–2106. [[CrossRef](#)] [[PubMed](#)]
5. Shu, X.; Chen, S.; Li, J.; Chen, Z.; Weng, L.; Jia, X.; Li, C. Highly effective binding of neutral dinitriles by simple pillar[5]arenes. *Chem. Commun.* **2012**, *48*, 2967–2969. [[CrossRef](#)]

6. Guo, D.-S.; Liu, Y. Supramolecular chemistry of p-sulfonatocalix[n]arenes and its biological applications. *Acc. Chem. Res.* **2014**, *47*, 1925–1934. [[CrossRef](#)]
7. Ma, X.; Zhao, Y. Biomedical applications of supramolecular systems based on host-guest interactions. *Chem. Rev.* **2015**, *115*, 7794–7839. [[CrossRef](#)]
8. Gui, J.-C.; Yan, Z.-Q.; Peng, Y.; Yi, J.-G.; Zhou, D.-Y.; Su, D.; Zhong, Z.-H.; Gao, G.-W.; Wu, W.-H.; Yang, C. Enhanced head-to-head photodimers in the photocyclodimerization of anthracenecarboxylic acid with a cationic pillar[6]arene. *Chin. Chem. Lett.* **2016**, *27*, 1017–1021. [[CrossRef](#)]
9. Li, J.; Shi, Q.; Han, Y.; Chen, C.-F. Complexation of 2,6-helic[6]arene and its derivatives with 1,1'-dimethyl-4,4'-bipyridinium salts and protonated 4,4'-bipyridinium salts: An acid–base controllable complexation. *Beilstein J. Org. Chem.* **2019**, *15*, 1795–1804. [[CrossRef](#)]
10. Han, X.-N.; Han, Y.; Chen, C.-F. Pagoda[4]arene and i-pagoda[4]arene. *J. Am. Chem. Soc.* **2020**, *142*, 8262–8269. [[CrossRef](#)]
11. Avestro, A.-J.; Belowicha, M.E.; Stoddart, J.F. Cooperative self-assembly: Producing synthetic polymers with precise and concise primary structures. *Chem. Soc. Rev.* **2012**, *41*, 5881–5895. [[CrossRef](#)] [[PubMed](#)]
12. Kakuta, T.; Yamagishi, T.-A.; Ogoshi, T. Stimuli-responsive supramolecular assemblies constructed from pillar[n]arenes. *Acc. Chem. Res.* **2018**, *51*, 1656–1666. [[CrossRef](#)] [[PubMed](#)]
13. Dong, S.; Yuan, J.; Huang, F. A pillar[5]arene/imidazolium [2]rotaxane: Solvent- and thermo-driven molecular motions and supramolecular gel formation. *Chem. Sci.* **2013**, *5*, 247–252. [[CrossRef](#)]
14. Wang, S.; Xu, Z.; Wang, T.; Xiao, T.; Hu, X.-Y.; Shen, Y.-Z.; Wang, L. Warm/cool-tone switchable thermochromic material for smart windows by orthogonally integrating properties of pillar[6]arene and ferrocene. *Nat. Commun.* **2018**, *9*, 1737. [[CrossRef](#)]
15. Jie, K.; Zhou, Y.; Li, E.; Huang, F. Nonporous adaptive crystals of pillararenes. *Acc. Chem. Res.* **2018**, *51*, 2064–2072. [[CrossRef](#)]
16. Wang, Y.; Xu, K.; Li, B.; Cui, L.; Li, J.; Jia, X.; Zhao, H.; Fang, J.; Li, C. Efficient separation of *cis*- and *trans*-1,2-dichloroethene isomers by adaptive biphen[3]arene crystals. *Angew. Chem. Int. Ed.* **2019**, *58*, 10281–10284. [[CrossRef](#)]
17. Li, J.; Han, Y.; Chen, C.-F. Recent advances in novel macrocyclic arenes. *Chin. J. Org. Chem.* **2020**, *40*, 3714. [[CrossRef](#)]
18. Ogoshi, T.; Kayama, H.; Yamafuji, D.; Aoki, T.; Yamagishi, T.A. Supramolecular polymers with alternating pillar[5]arene and pillar[6]arene units from a highly selective multiple host–guest complexation system and monofunctionalized pillar[6]arene. *Chem. Sci.* **2012**, *3*, 3221–3226. [[CrossRef](#)]
19. Yu, G.; Han, C.; Zhang, Z.; Chen, J.; Yan, X.; Zheng, B.; Liu, S.; Huang, F. Pillar[6]arene-based photoresponsive host–guest complexation. *J. Am. Chem. Soc.* **2012**, *134*, 8711–8717. [[CrossRef](#)]
20. Li, C.; Shu, X.; Li, J.; Fan, J.; Chen, Z.; Weng, L.; Jia, X. Selective and effective binding of pillar[5,6]arenes toward secondary ammonium salts with a weakly coordinating counteranion. *Org. Lett.* **2012**, *14*, 4126–4129. [[CrossRef](#)]
21. Shi, Q.; Han, Y.; Chen, C.-F. Complexation between (O-methyl)6-2,6-helic[6]arene and tertiary ammonium salts: Acid/base- or chloride-ion-responsive host–guest systems and synthesis of [2]rotaxane. *Chem. Asian J.* **2017**, *12*, 2576–2582. [[CrossRef](#)] [[PubMed](#)]
22. Zhang, G.-W.; Li, P.-F.; Wang, H.-X.; Han, Y.; Chen, C.-F. Complexation of racemic 2,6-helic[6]arene and its hexamethyl substituted derivative with quaternary ammonium salts, N-heterocyclic salts, and tetracyanoquinodimethane. *Chem. Eur. J.* **2017**, *23*, 3735–3742. [[CrossRef](#)] [[PubMed](#)]
23. Zhang, G.-W.; Li, P.; Meng, Z.; Wang, H.-X.; Han-Xiao, W.; Chen, C.-F. Triptycene-based chiral macrocyclic hosts for highly enantioselective recognition of chiral guests containing a trimethylamino group. *Angew. Chem. Int. Ed.* **2016**, *55*, 5304–5308. [[CrossRef](#)] [[PubMed](#)]
24. Li, J.; Han, X.-N.; Zhou, H.-Y.; Han, Y.; Chen, C.-F. Helic[1]triptycene[3]arene: Synthesis, complexation, and formation of [2]rotaxane shuttle. *J. Org. Chem.* **2020**, *85*, 11465–11474. [[CrossRef](#)]
25. Witiak, D.T.; Loper, J.T.; Ananthan, S.; Almerico, A.M.; Verhoef, V.L.; Filppi, J.A. Mono and bis(bioreductive) alkylating agents: Synthesis and antitumor activities in a B16 melanoma model. *J. Med. Chem.* **1989**, *32*, 1636–1642. [[CrossRef](#)]
26. Thordarson, P. Determining association constants from titration experiments in supramolecular chemistry. *Chem. Soc. Rev.* **2010**, *40*, 1305–1323. [[CrossRef](#)]
27. Frisch, M.J.; Trucks, G.W.; Schlegel, H.B.; Scuseria, G.E.; Robb, M.A.; Cheeseman, J.R.; Scalmani, G.; Barone, V.; Mennucci, B.; Petersson, G.A.; et al. *Gaussian 09, Revision A.02*; Gaussian, Inc.: Wallingford, CT, USA, 2009.
28. Castellano, R.K. Progress toward understanding the nature and function of C-H ... O interactions. *Curr. Org. Chem.* **2004**, *8*, 845–865. [[CrossRef](#)]
29. Lu, T.; Chen, F. Multiwfn: A multifunctional wavefunction analyzer. *J. Comput. Chem.* **2012**, *33*, 580–592. [[CrossRef](#)]